DALTON
FULL PAPER

# Structural evidence for the facile chelate-ring opening reactions of novel platinum(II)–pyridine carboxamide complexes †

**Junyong Zhang,[a] Qin Liu,[a,b] Chunying Duan,[a] Ying Shao,[a] Jian Ding,[c] Zehong Miao,[c] Xiao-Zeng You[a] and Zijian Guo*[a]**

[a] *State Key Laboratory of Coordination Chemistry, Coordination Chemistry Institute, Nanjing University, 210093 Nanjing, P.R. China. E-mail: zguo@netra.nju.edu.cn*
[b] *Department of Food Sciences and Engineering, Nanjing College of Economics, 210003 Nanjing, P.R. China*
[c] *Division of Anti-tumor Pharmacology, State Key Laboratory for New Drug Research, Shanghai Institute of Materia Medica, Shanghai Institutes of Biological Sciences, Chinese Academy of Sciences, Shanghai 200031, P.R. China*

***Received 14th September 2001, Accepted 14th November 2001***
***First published as an Advance Article on the web 21st January 2002***

The design of Pt(II) complexes with novel structural features is of great relevance in the search for new anticancer agents with innovative chemical and biological properties. In this work we have synthesised and structurally characterised three novel Pt(II) complexes with a pyridine carboxamide ligand (HL). The X-ray structural analysis shows that complex **1**, [Pt(L-*N*, *N'*)$_2$] crystallises in space group *C*2, while complex **2**, [Pt(L-*N,N'*)(L-*N*)Cl] crystallises in space group $P2_1$. ESMS and $^1$H NMR data show that one of the two ligands in complex **1** undergoes a fast ring-opening reaction to give complex **2** in the presence of $Cl^-$. Complex **2** demonstrated notable activity against human and murine leukemia cells (HL-60 and P388), but rather weak potency against lung adenocarcinoma A-549. However, complex **1** was found to be basically inactive against the above cell lines. This work provides new examples in the design of platinum compounds that can be activated *in vivo* by biological anions.

## Introduction

The search for novel platinum and other metal-based anticancer drugs with better efficacy and lower toxicity has been going on since the discovery of the anti-proliferation activity of cisplatin in the 1960s.[1] It is expected that new metallotherapeutic agents will be discovered through the efforts of chemists from the medicinal inorganic chemistry field.[2–4]

Platinum compounds are currently amongst the most widely used drugs for the treatment of cancer.[5,6] However, their severe toxicity such as nephrotoxicity and neurotoxicity, coupled with drug resistance which develops within patients after initial treatments, have greatly limited their wider clinical application.[5] Although several new-generation platinum-based drugs that have reduced toxicity have recently been introduced into clinical usage, patients develop cross-resistance to them due to their structural similarity to cisplatin. Therefore, compounds with novel structural features are required which could potentially provide different biological properties.

Among the new design strategies developed, the incorporation of pyridine-derived ligands into platinum(II) complexes has resulted in the discovery of ZD0473 (former JM473 or AM473), *cis*-[$PtCl_2(NH_3)$(2-MePy)],[7,8] which is under phase I clinical evaluation.[9] The steric hindrance of the 2-methylpyridine ligand in ZD0473 dramatically slows down the hydrolysis rate of the chlorine in the *cis* position and the reactivity towards cellular thiols such as glutathione.[10] Recent data show that ZD0473 forms a specific adduct with duplex DNA.[11] Farrell *et al.*[12–16] have examined a series of platinum(II) complexes with N-containing heterocyclic ligands such as pyridine, thiazole and quinoline and found some of them to possess potent anticancer activities.

Platinum(II) complexes with a [$PtN_4$] structure are generally considered anticancer inactive since they cannot readily bind to DNA due to the high thermodynamic stability of the Pt–N bonds.[17] For example, a half-life of *ca*. 23 years has been estimated for direct $NH_3$ exchange in $[Pt(NH_3)_4]^{2+}$ at 25 °C in aqueous $NH_3$ solution.[18] However, recent examples have illustrated that the Pt–N bond can become labile and be displaced by $Cl^-$ when a phosphorus atom (part of a ligand with a strong *trans* effect) is introduced at the *trans* position to the nitrogen atoms.[19–21] The chelate ring-opened Pt(II) aminophosphine complexes bind rapidly and strongly to thymine and uracil under physiological conditions.[22] In this work we have synthesised three Pt(II) complexes with a pyridine carboxamide chelating ligand, two of them have been structurally characterized by X-ray diffraction. Our data demonstrate that the presence of a bulky group on the amide nitrogen facilitates the transformation of the bis-chelate complex to its ring-opened counterpart in solution.

## Experimental

Solvents such as pyridine, ethanol and acetone were all analytical reagents and used as received. $K_2[PtCl_6]$ and 4-methylaniline were purchased from the First Reagent Factory of Shanghai, and 2-pyridinecarboxylic acid from Sigma. $K_2[PtCl_4]$ was synthesized by the reduction of $K_2[PtCl_6]$ using hydrazine following the standard procedure.[23]

The infrared spectra were recorded on a Bruker VECTOR22 spectrometer as KBr pellets (4000–500 $cm^{-1}$). The $^1$H and 2D

† Electronic supplementary information (ESI) available: the aromatic region of the 2D COSY NMR spectrum of HL (in $CDCl_3$, 298 K); calculated mass spectra of peaks 1, 5, 6′, 9, 11, 12; cytotoxic activity of cisplatin against selected tumor lines. See http://www.rsc.org/suppdata/dt/b1/b108378n/

DOI: 10.1039/b108378n

COSY NMR spectra were recorded on a Bruker DRX-500 spectrometer using standard pulse sequences. Elementary analysis was performed on a Perkin-Elmer 240C analytical instrument.

Electrospray mass spectra were recorded using an LCQ electron spray mass spectrometer (ESMS, Finnigan) by loading 1.0 μl of solution into the injection valve of the LCQ unit and then injecting into the mobile phase solution (50% of aqueous methanol) that was carried through the electrospray interface into the mass analyzer at a rate of 200 μl $min^{-1}$. The voltage employed at the electrospray needles was 5 kV, and the capillary was heated to 200 °C. A maximum ion injection time of 200 ms along with 10 scans was set. Positive and negative ion mass spectra were obtained. The predicted isotope distribution patterns for each of the complexes were calculated using the Isopro 3.0 program.[24]

## Preparations

***N*-(4-Methylphenyl)-2-pyridinecarboxamide (HL).** This ligand was prepared following a reported procedure for a carboxamide compound.[25,26] A mixture of 2-pyridinecarboxylic acid (1.231 g, 10 mmol) and 4-methylaniline (1.072 g, 10 mmol) in 10 ml of pyridine was heated with stirring to 100 °C in an oil bath. Then, triphenylphosphite (3.1 g, 10 mmol) was added slowly to the mixture. The mixture was further stirred for 3 h at 100 °C, then cooled to room temperature. The solvent was removed by rotary evaporation to give a pale brown solution from which colorless crystals were obtained. Yield: 70% [Found: C: 73.47; H: 5.67; N: 13.19. Calc. for $C_{13}H_{12}N_2O$: C: 73.58; H: 5.66; N: 13.21%]. IR: $\nu_{NH}$: 3320 $cm^{-1}$, $\nu_{CO}$: 1675 $cm^{-1}$.

**[$PtL_2$] (1), [$PtL_2Cl$] (2) and [PtLCl] (3).** These three complexes were prepared as follows. An aqueous solution of $K_2PtCl_4$ (0.1 mmol, 41.5 mg, 2 ml) was mixed with an acetone solution of HL in 1 : 2 molar ratio (0.2 mmol, 42.5 mg, 2 ml). The mixture was then refluxed for 2 h. A yellowish precipitate formed upon cooling to room temperature, and this was collected by filtration. The yellow precipitate (38.4 mg) was recrystallised from the mixed solvents acetone and water, and orange crystals suitable for X-ray determination were obtained and identified as complex **1** and yellow crystals as complex **2** and they were mechanically separated [Found: **1**, C: 50.43 H: 3.60, N: 9.75. Calc. for $C_{26}H_{22}N_4O_2Pt$: C: 50.52, H: 3.56, N: 9.68%. **2**, C: 47.70, H: 3.57, N: 8.61. Calc. for $C_{26}H_{23}ClN_4O_2Pt$: C: 47.73, H: 3.51, N: 8.56%]. IR: **1**, $\nu_{NH}$: ≈3447 $cm^{-1}$, $\nu_{CO}$: 1633 $cm^{-1}$; **2**, $\nu_{NH}$: ≈3447 $cm^{-1}$, $\nu_{CO}$: 1676 $cm^{-1}$, 1650 $cm^{-1}$. The mother-liquor, which contains 2 molar equivalents of KCl formed during the reaction, was left for slow evaporation, giving complex **3** [Found: C: 32.6, H: 2.57, N: 5.79. Calc. for $C_{13}H_{12}Cl_2N_2OPt$: C: 32.64, H: 2.53, N: 5.86%].

## Density determination

The density of one of the crystals of **2** was determined as 0.823 mg $mm^{-3}$ using buoyancy methods from the mixed solvents water and ethanol, in which **2** is nearly insoluble.

## Ring-opening experiments in the presence of LiCl followed by $^1$H NMR and ESMS

For NMR experiments, solutions of LiCl in $CD_3OD$ (50 mM) and complex **1** (6.25 mM) in $CD_3OD$ were prepared separately. Immediately after the mixing of 0.1 ml LiCl with 0.4 ml complex **1**, $^1$H NMR spectra were recorded and monitored for 48 h.

Samples for ESMS experiments were prepared as follows. Complex **1** was dissolved in $CHCl_3$ to make a 2 mg $ml^{-1}$ solution and then diluted with $CH_3OH$ to 1 mg $ml^{-1}$ for the measurement. The ESMS spectra of complex **1** and LiCl in $CDCl_3/CD_3OD$ were recorded immediately after the addition of LiCl and followed for 3 days.

## Crystallography

Table 1 summarizes the crystal data, data collection, structural solution and refinement parameters for complexes **1** and **2**. The crystal of **1** was an orange block that was mounted on a glass fiber and used for data collection. Cell constants and an orientation matrix for data collection were obtained by least-squares refinement of diffraction data from 34 reflections in the range $7.10 < \theta < 14.2$ on a Siemens P4 four-circle diffractometer. Data were collected at 293 K using monochromated Mo-Kα radiation and the $\omega$–$2\theta$ scan technique with a variable scan speed 5.0–50.0 $min^{-1}$ in $\omega$ and corrected for Lorentz and polarization effects. An empirical absorption correction was made ($\psi$-scan). The structure was solved by direct-methods which revealed the position of all non-hydrogen atoms and refined on $F^2$ by a full-matrix least-squares procedure using anisotropic displacement parameters. All the hydrogen atoms were placed in their calculated positions (C–H = 0.93 Å, N–H = 0.86 Å) with $U_{iso}$ = 1.2 $U_{eq}$.

A pale yellow prism of **2** of approximate dimensions 0.15 × 0.10 × 0.10 mm was used for data collection and cell parameter determination on an Enraf-Nonius CAD-4 diffractometer with the $\omega$–$2\theta$ scan mode. The data were also corrected for Lorentz and polarization effects and an absorption correction was made using the $\psi$-scan method. The structure was solved by Patterson methods and completed by iterative cycles of least-squares refinement and $\Delta F$-syntheses. H-Atoms were located in their calculated positions and treated as riding on the atoms to which they are attached. Only the Pt and Cl atoms were refined anisotropically. The occupancies for all the atoms are 50% due to their disorder. The density of crystal **2** was 0.792 mg $mm^{-3}$ which is close to the value obtained from the density determination experiment (0.823 mg $mm^{-3}$). All calculations were carried out using the SHELXTL program.[27]

CCDC reference numbers 170947 and 170948.

See http://www.rsc.org/suppdata/dt/b1/b108378n/ for crystallographic data in CIF or other electronic format.

## Cytotoxicity assay

Tumor cell lines were grown in RPMI-1640 medium supplemented with 10% (vol/vol) calf serum, 2 mmol $L^{-1}$ glutamine, 100 U $mL^{-1}$ penicillin (U = 1 unit of activity), and 100 μg $mL^{-1}$ streptomycin (GIBCO, Grand Island, NY) at 37 °C under 5% $CO_2$. Cells in 100 μL culture medium were seeded into 96-well plates (Falcon, CA).

For murine leukemia P-388 and human leukemia HL-60 cells, the microculture MTT [3-(4,5-dimethylthiazol-2-yl)-2,5-diphenyl-2*H*-tetrazolium bromide] assay[28] was conducted as follows. The cells were treated in triplicate with grade concentrations of complexes **1**, **2** and the reference drug cisplatin at 37 °C for 48 h. A 20 μL aliquot of MTT solution (5 mg $mL^{-1}$) was added directly to all the appropriate wells. The culture was then incubated for 4 h. A 50 μl aliquot of 50% SDS [$CH_3(CH_2)_{11}OSO_3Na$]–5% isobutyl alcohol–0.01moL $mL^{-1}$ hydrochloride solution was added. After the plates were incubated overnight, the optical densities were read on a plate reader (model VERSA Max, Molecular Devices) at 570 nm.

For human hepatoma BEL-7402 and lung adenocarcinoma A-549 cells, the growth inhibition was analysed by the sulforhodamine B(SRB) assay.[29] Simply, following the treatment with complexes **1** and **2** for 72 h, the cell cultures were fixed with 10% trichloroacetic acid and incubated for 60 min at 4 °C. Then, the plates were washed and dried. SRB solution (0.4% wt/vol in 1% acetic acid) was added and the culture was incubated for an additional 15 min. After the plates were washed and dried, bound stain was solubilized with Tris buffer, and the optical densities were read on the same plate reader at 515 nm. The growth inhibitory rate of treated cells was calculated by $(OD_{control} - OD_{test})/OD_{control} \times 100\%$.

**Table 1** Crystal data and structure refinement for complexes **1** and **2**

| | **1** | **2** |
|---|---|---|
| Empirical formula | $C_{26}H_{22}N_4O_2Pt$ | $C_{26}H_{23}ClN_4O_2Pt$ |
| Formula weight | 617.57 | 654.02 |
| $T$/K | 293(2) | 293(2) |
| Crystal size/mm | 0.30 × 0.15 × 0.15 | 0.15 × 0.10 × 0.10 |
| Crystal habit, colour | Block, orange | Prism, yellow |
| Crystal system | Monoclinic | Monoclinic |
| Space group | $C2$ | $P2_1$ |
| $a$/Å | 13.7781(11) | 9.459(5) |
| $b$/Å | 12.8683(15) | 13.394(5) |
| $c$/Å | 6.2537(13) | 10.898(5) |
| $\beta$/° | 95.229(11) | 96.82(5) |
| $V$/Å$^3$ | 1104.2(3) | 1370.9(11) |
| $Z$ | 2 | 1 |
| Calculated density/Mg m$^{-3}$ | 1.857 | 0.792 |
| $\mu$/mm$^{-1}$ | 6.386 | 2.621 |
| Reflections collected | 1264 | 2675 |
| Independent reflections | 1115 ($R_{int}$ = 0.0290) | 2517 ($R_{int}$ = 0.0186) |
| Goodness-of-fit on $F^2$ | 1.149 | 1.154 |
| Final $R$ indices [$I > 2\sigma(I)$] | $R1$ = 0.0599, $wR2$ = 0.1420 | $R1$ = 0.0508, $wR2$ = 0.1410 |
| Largest difference peak, hole/e Å$^{-3}$ | 1.889, −0.838 | 1.168, −0.524 |

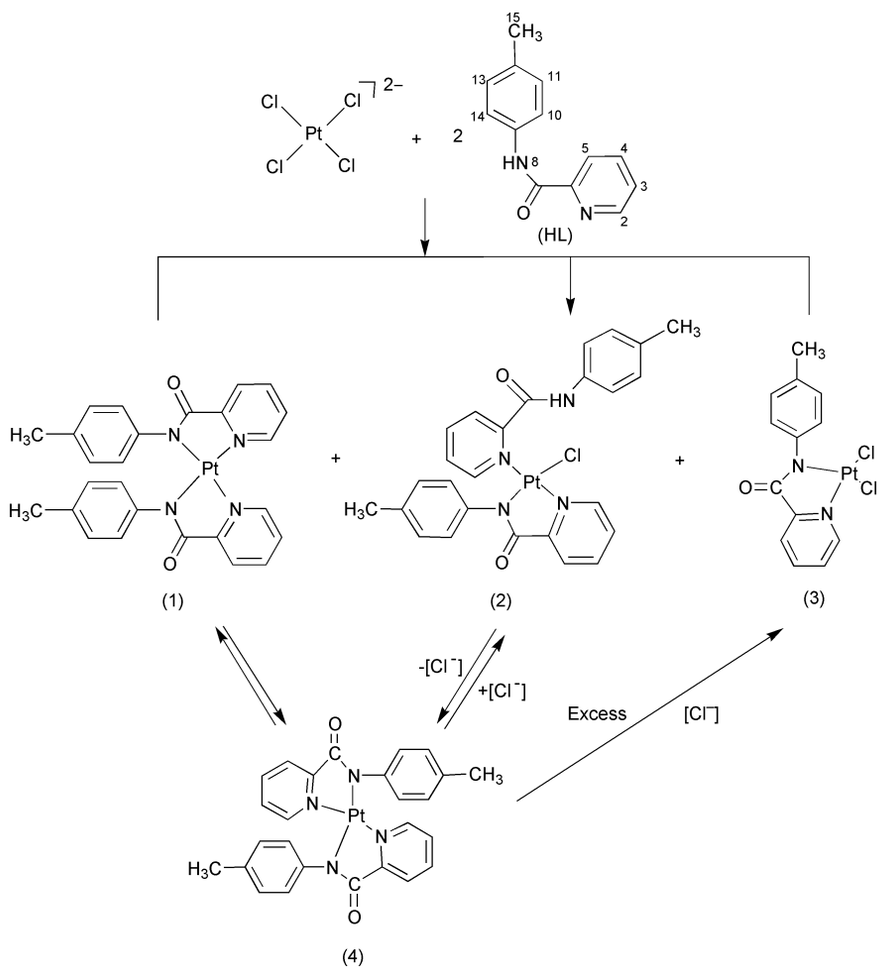


**Scheme 1**

## Results and discussion

Scheme 1 outlines the reaction of $K_2[PtCl_4]$ with HL in 1 : 2 molar ratio that gives complexes **1**, **2** and **3**. The complexes were separated mechanically and characterized by IR, $^1$H NMR, ESMS and X-ray diffraction.

### Crystallography

The molecular structure and numbering scheme for complex **1** is shown in Fig. 1. Selected bond lengths and angles for complexes **1** and **2** are listed in Tables 2 and 3, respectively. As can be seen from Fig. 1, Pt(II) in **1** adopted a distorted square-planar geometry coordinated by two equivalent pyridine nitrogen atoms [N(1) and N(1A)] and two amide N atoms [N(8) and N(8A)] from two ligands arranged in a *cis* configuration. The mean deviation from the $PtN_4$ plane [Pt(1), N(1), N(8), N(1A) and N(8A)] is 0.003 Å. The approximately square-planar coordination of the Pt(II) atom generates two five-numbered rings. The torsion angles Pt(1)–N(1)–C(6)–C(7) and Pt(1)–N(8)–C(7)–C(6) are −1.1° and 14.4°, respectively. As can be noted the bond length of Pt(1)–N(8) is in the expected region for a Pt(II)–amide bond, while the Pt(1)–N(1) bond length

**Table 2** Selected bond lengths (Å) and angles (°) for **1**

| | | | |
|---|---|---|---|
| Pt(1)–N(1) | 2.081(6) | Pt(1)–N(8) | 2.021(7) |
| N(8)–C(9) | 1.453(7) | N(8)–C(7) | 1.346(15) |
| C(7)–C(6) | 1.474(11) | C(7)–O(7) | 1.242(15) |
| N(1)–C(2) | 1.348(6) | C(2)–C(3) | 1.393(6) |
| C(3)–C(4) | 1.395(5) | C(4)–C(5) | 1.393(5) |
| C(5)–C(6) | 1.395(5) | C(6)–N(1) | 1.351(6) |
| N(8)–Pt(1)–N(8A) | 92.6(4) | N(8)–Pt(1)–N(1) | 79.5(2) |
| N(8A)–Pt(1)–N(1) | 172.2(3) | N(1A)–Pt(1)–N(1) | 108.3(3) |
| C(9)–N(8)–C(7) | 115.2(7) | O(7)–C(7)–C(6) | 114.1(10) |
| C(9)–N(8)–Pt(1) | 128.4(6) | C(2)–N(1)–Pt(1) | 122.8(4) |
| N(8)–C(7)–C(6) | 113.5(9) | Pt(1)–N(8)–C(7) | 115.4(6) |

Symmetry code: A $-x + 2$, $y$, $-z + 1$.

**Table 3** Selected bond lengths (Å) and angles (°) for **2**[a]

| | | | |
|---|---|---|---|
| Pt(1)–N(1) | 2.080(7) | Pt(1)–N(8′) | 1.968(9) |
| Pt(1)–N(1′) | 2.056(7) | Pt(1)–Cl(1) | 2.336(3) |
| N(1)–C(2) | 1.299(12) | N(1)–C(6) | 1.287(10) |
| C(2)–C(3) | 1.388(13) | C(3)–C(4) | 1.375(14) |
| C(4)–C(5) | 1.415(15) | C(5)–C(6) | 1.346(12) |
| C(6)–C(7) | 1.534(11) | C(7)–N(8) | 1.330(10) |
| N(8)–C(9) | 1.404(10) | C(7)–O(7) | 1.261(10) |
| C(6′)–C(7′) | 1.483(12) | C(7′)–N(8′) | 1.273(11) |
| N(8′)–Pt(1)–N(1′) | 79.4(3) | N(8′)–Pt(1)–N(1) | 97.2(3) |
| N(1′)–Pt(1)–N(1) | 176.6(3) | N(8′)–Pt(1)–Cl(1) | 175.4(2) |
| N(1′)–Pt(1)–Cl(1) | 96.3(2) | N(1)–Pt(1)–Cl(1) | 87.1(2) |
| C(9)–N(8)–C(7) | 126.7(7) | O(7)–C(7)–C(6) | 118.7(7) |
| C(9′)–N(8′)–C(7′) | 117.1(8) | O(7′)–C(7′)–C(6′) | 114.4(8) |
| C(7′)–N(8′)–Pt(1) | 120.1(7) | Pt(1)–N(1′)–C(2′) | 127.6(6) |
| C(9′)–N(8′)–Pt(1) | 122.6(6) | N(8′)–C(7′)–C(6′) | 112.1(8) |

[a] Primes are used to distinguish atoms belonging to two different ligands.

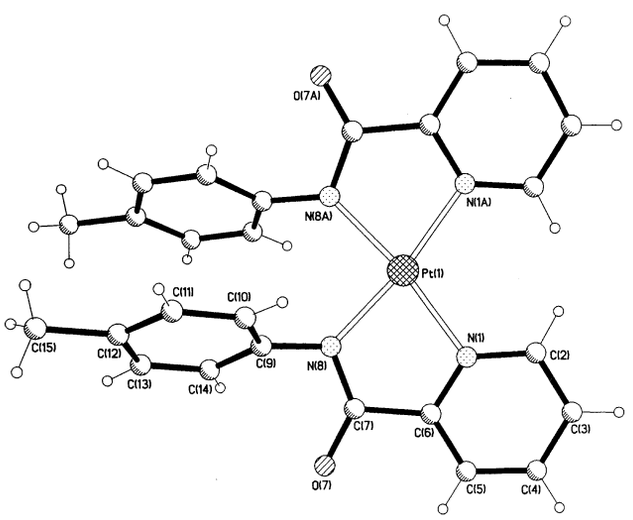


**Fig. 1** An ORTEP[27] view of complex **1** (symmetry code A $-x + 2$, $y$, $-z + 1$).

(2.081(6) Å) is 0.06–0.1 Å longer than the normal values found for Pt–N. This may be due to the different electron-donating abilities of amide N and pyridine N atoms.[30] The C(9)–N(8) bond distance is longer than that in [Cu(bpb)($H_2O$)] [1.398(3) Å][31] and Ni(bpb) [1.412(3) Å] (bpb = 1,2–bis(2–pyridinecarboxamido)benzene).[32] The phenyl rings are not in the $PtN_4$ plane. The dihedral angle between the phenyl ring **I** [C(9)–C(14)] and the $PtN_4$ plane (identified as **C**) is 64.6(4)° and the angle between the two phenyl rings is 8.1(3)°. This conformation may be stabilized by the π–π stacking interactions between the two phenyl rings, with the shortest interplanar atom–atom separation being *ca.* 3.04 Å [C(9) ··· C (9A)].

Since the density of complex **2** determined by the buoyancy method was 0.823 mg $mm^{-3}$, the value of $Z$ was confined to 1

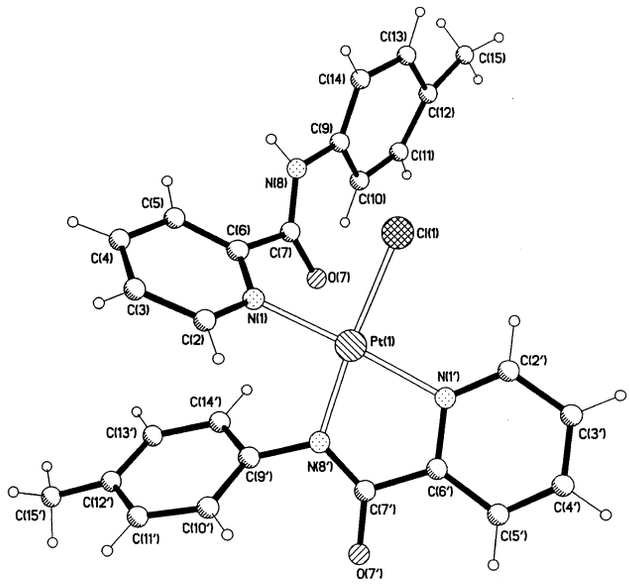


**Fig. 2** An ORTEP view of complex **2**.

instead of 2. Fig. 2 shows the molecular structure and numbering scheme of complex **2** in which the Pt(II) is coordinated in a square planar geometry composed of three nitrogen atoms and a chloride anion. It is notable that in complex **2** the two ligands are *trans* to each other (*i.e.* N1 is *trans* to N1′). This suggests that a *cis–trans* isomerization reaction has occurred during the conversion from complex **1** to **2**. The mean deviation from the $PtN_3Cl$ plane [Pt(1), N(1), N(8′), N(1′) and Cl(1)] is 0.0177 Å. The coordination of the Pt(II) atom also generates a five-membered ring and the torsion angles Pt(1)–N(8′)–C(7′)–C(6′) and Pt(1)–N(1′)–C(6′)–C(7′) are 3.9(10)° and 9.7(9)°, respectively. The Pt(1)–N(8′) and Pt(1)–N(1′) bond lengths are shorter than the corresponding Pt–N bonds in **1** and come close to the average value. The Pt–Cl bond in **2** is similar to the normal value expected for $Cl^-$ *trans* to a pyridine N [2.336(3) Å] and the N(8′)–Pt(1)–Cl(1) angle is in agreement with linear coordination [175.4(2)°].

The ring-closed ligand in complex **2** adopts a configuration in which the N(1′) atom is *cis* to N(8′). The torsion angle N(8′)–C(7′)–C(6′)–N(1′) is −9.2(11)°. Rotation of the amide group by 180° about the C(7)–C(6) bond places the amide nitrogen atom and pyridine nitrogen on different sides, thus giving a ring-opened ligand in which the torsion angle N(8)–C(7)–C(6)–N(1) is −135.7(8)°. Deprotonation of the ring-closed ligand makes the N(8′)–C(7′) bond shorter than that of N(8)–C(7) in the ring-opened ligand, indicating some double-bond character in N(8′)–C(7′). The ring orientation in complex **2** can be defined as follows. Labeling the phenyl ring in the ring-closed ligand as **I** [C(9′)–C(14′)], the pyridyl ring in the ring-opened ligand as **II** [N(1)–C(6)], the phenyl ring in the ring-opened one as **III** [C(9)–C(14)], and the best metal coordination plane **C** ($PtN_3Cl$), it is found that the ligands are oriented differently. The dihedral angles between best planes **C–I**, **C–II**, **C–III**, **I–II**, **I–III** and **II–III** are 62.84(3)°, 64.47(2)°, 61.02(2)°, 38.58(4)°, 78.39(2)° and 69.47(2)°, respectively.

## ESMS Studies

The ESMS spectra of **1**, **2** and **3** were recorded in $CH_3Cl$/MeOH solution. Fig. 3a shows the ESMS spectrum of complex **1**. As can be seen, there are four major species and the highest peak (peak 1) has an $m/z$ value of 618.3 and can be assigned to positively charged $[PtL_2]^+$ (Fig. 3b). The $m/z$ value and isotopic distribution of peak 2 (719.8) corresponded to complex $[PtL_2Na_3CH_3OH]^+$, peak 3 (1235.7) to $[Pt_2L_4]^+$ and peak 4 (1256.9) to $[Pt_2L_4Na]^+$. The calculated molecular mass and the isotopic distribution of these peaks match perfectly with the

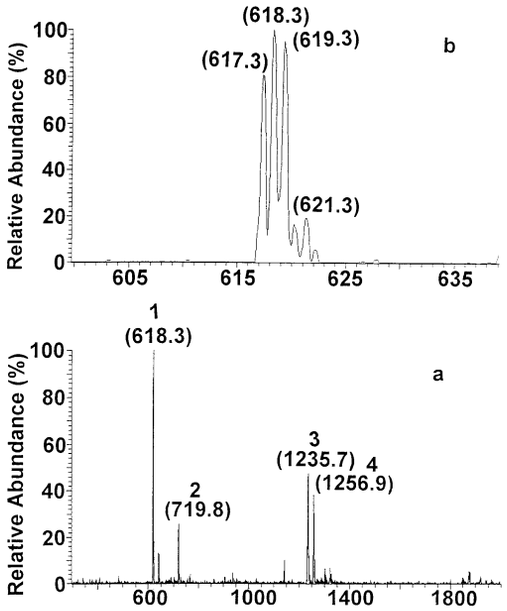


**Fig. 3** (a) The ESMS spectrum of complex **1** in $CHCl_3/CH_3OH$. (b) The expanded spectrum of peak 1 which is assigned to $[PtL_2]^+$.

corresponding formulae (see Fig. S2). The data suggest that complex **1** in solution was the same as in the solid state and that both ligands exist in the chelated form.

The ESMS spectrum of complex **2** is shown in Fig. 4a. There

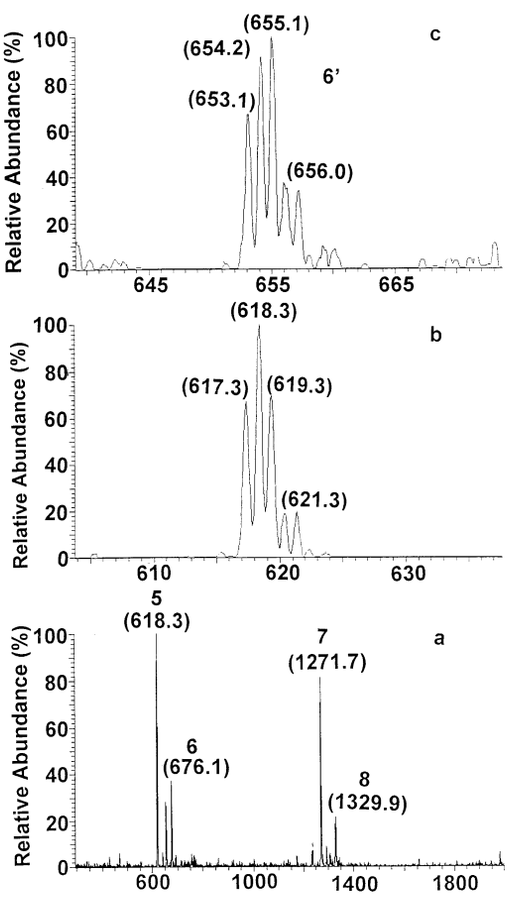


**Fig. 4** (a) The ESMS spectrum of complex **2** in $CHCl_3/CH_3OH$. (b) The expanded spectrum of peak 5 ($[PtL_2]^+$). (c) The expanded spectrum of peak 6′ ($[PtL_2Cl–H]^+$) and 6 ($[PtL_2ClNa]^+$).

are 5 major species detected in the spectrum, among them, the highest peak (peak 5) has an *m*/*z* value of 618.3 (Fig. 4b) which can also be assigned to positively charged $[PtL_2]^+$, which is identical to peak 1 in Fig. 3b. The other peaks can be assigned

**Table 4** Observed and calculated molecular masses of the complexes **1**, **2**, **3** and of compound **1** + LiCl after a few days

| Peak | Compound | Observed mass[a] | Calculated mass |
|---|---|---|---|
| 1 | $[PtL_2]^+$ | 617.3–622.2 | 617.6 |
| 2 | $[PtL_2Na_3CH_3OH]^+$ | 718.7–722.7 | 718.6 |
| 3 | $[Pt_2L_4]^+$ | 1232.8–1239.7 | 1234.1 |
| 4 | $[Pt_2L_4Na]^+$ | 1255.0–1262.1 | 1257.1 |
| 5 | $[PtL_2]^+$ | 617.3–622.3 | 617.6 |
| 6 | $[PtL_2ClNa]^+$ | 675.1–681.1 | 676.0 |
| 6′ | $[PtL_2Cl - H]^+$ | 653.1–659.1 | 654.0 |
| 7 | $[Pt_2L_4Cl]^+$ | 1269.0–1277.9 | 1270.6 |
| 8 | $[Pt_2L_4Cl_2Na]^+$ | 1326.9–1335.9 | 1330.0 |
| 9 | $[PtLCl_2]^-$ | 475.5–480.1 | 478.3 |
| 10 | $[PtL_2Na]^+$ | 640.7–644.6 | 640.6 |
| 11 | $[PtL_2Cl]^+$ | 654.7–658.7 | 655.0 |
| 12 | $[PtLCl_2]^-$ | 475.3–481.1 | 478.3 |

[a] The peaks are separated by 1 *m*/*z* in the mass region indicated.

to $[PtL_2ClNa]^+$ (peak 6, 676.1), $[Pt_2L_4Cl]^+$ (peak 7, 1271.7) and $[Pt_2L_4Cl_2Na]^+$ (peak 8, 1329.9), respectively. The expanded spectrum of peak 6′ is shown in Fig. 4c. These data suggest that in solution complex **2** can easily undergo ring-closure to give complex **1** ($[PtL_2]^+$).

Fig. 5a shows the ESMS spectrum of complex **3**. The major

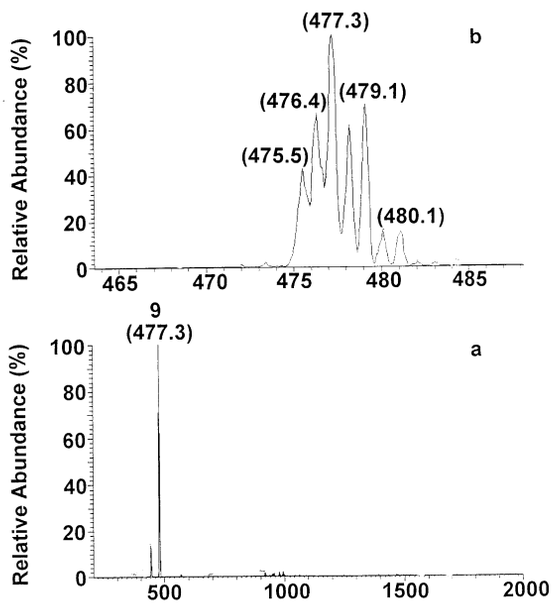


**Fig. 5** (a) The ESMS spectrum of complex **3** in $CHCl_3/CH_3OH$. (b) The expanded spectrum of peak 9 ($[PtLCl_2]^-$).

peak detected (peak 9, 477.3, Fig. 5b) can be assigned to negatively charged $[PtLCl_2]^-$. The ESMS data of the complexes are summarised in Table 4, together with the calculated values.

Fig. 6a shows the ESMS spectrum of a mixture of complex **1** and LiCl, which was recorded immediately after mixing (about 2 min). As can be seen, the highest peak has a *m*/*z* value of 656.7 (peak 11, Fig. 6b) and can be assigned to positively charged $[PtL_2Cl]^+$, which is similar to peak 6′ (Fig. 4c) although peak 6′ is less resolved. However, the peak (618.3) representing the double ring-closed complex **1** has nearly disappeared, and a small amount of $[PtL_2Na]^+$ (peak 10, 641.6) exists in the spectrum (Fig. 6a). This suggests that complex **1** undergoes a facile chelate-ring opening reaction in the presence of excess $Cl^-$ to give complex **2** and the process is completed within a few minutes. About 2 days after mixing, complex **3** appeared in the ESMS spectrum. Fig. 7a shows the spectrum of the mixture recorded 3 days after mixing. The highest peak has a *m*/*z* value of 477.2 (peak 12, Fig. 7b) and can be attributed to negatively charged $[PtLCl_2]^-$, which is identical to peak 9 (Fig. 5b). This

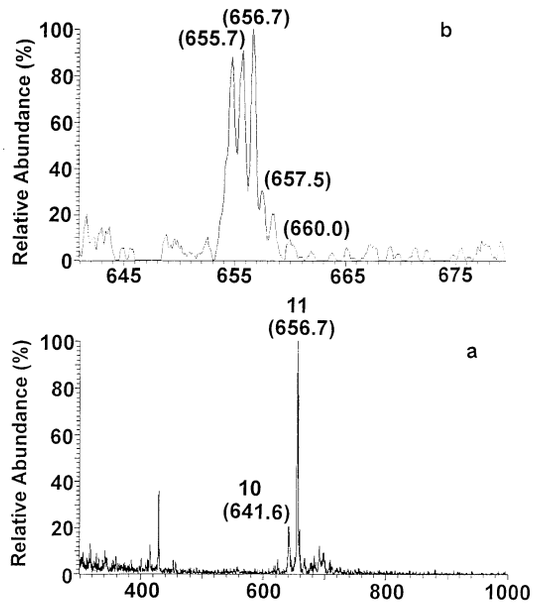


**Fig. 6** (a) The ESMS spectrum of complex **1** + LiCl in $CHCl_3$/$CH_3OH$ immediately after mixing (about 2 min). (b) The expanded spectrum of peak 11 ($[PtL_2Cl]^+$).

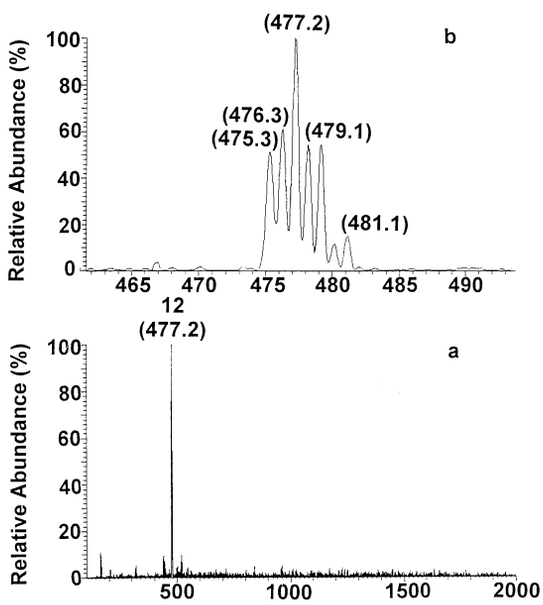


**Fig. 7** (a) The ESMS spectrum of complex **1** + LiCl in $CHCl_3$/$CH_3OH$ 3 days after mixing. (b) The expanded spectrum of peak 12 ($[PtLCl_2]^-$).

suggests that the ring-opened ligand in complex **2** can be further replaced by $Cl^-$ to give rise to complex **3** instead of double ring-opened complexes. This is also confirmed by NMR spectroscopy.

## NMR spectroscopy

The $^1H$ NMR spectrum of free HL shows 6 aromatic signals at 8.68d, 7.58m, 7.99t, 8.26d, 7.66d, and 7.22d ppm. These can be assigned to the proton resonances of 2, 3, 4, 5, 10 + 14, 11 + 13, respectively, according to the connectivities in the 2D COSY spectrum (Fig. S1) (see Scheme 1 for the numbering of the positions in HL and complex **2**).

Due to the fast conversion of complex **2** into **1** in the absence of $Cl^-$ as observed by ESMS, the $^1H$ NMR spectra of complexes **1** and **2** in $CDCl_3$/$CD_3OD$ are identical; two sets of signals are observed, suggesting the inequivalency of the two ligands. Because the ring-closure of complex **2** may give the *trans* isomer of complex **1** (complex **4**, Scheme 1) and as some

**Table 5** $^1H$ NMR chemical shifts of complex **2**

| $^1H$ resonance | Chemical shift (ppm) |
|---|---|
| 2 | 8.79d |
| 3 | 7.22t |
| 4 | 7.78t |
| 5 | 7.72d |
| 10 + 14 | 7.78t |
| 11 + 13 | 7.22t |
| 2′ | 9.31d |
| 3′ | 7.58t |
| 4′ | 8.13t |
| 5′ | 7.93d |
| 10′ + 11′ + 13′ + 14′ | 6.84d, 6.81d |

of the $^1H$ signals are extremely overlapped, detailed assignments cannot be made. The addition of $Cl^-$ to a fresh solution of complex **1** gives complex **2** as shown by ESMS, however, the process is too fast to be followed by $^1H$ NMR. Fig. 8 shows a

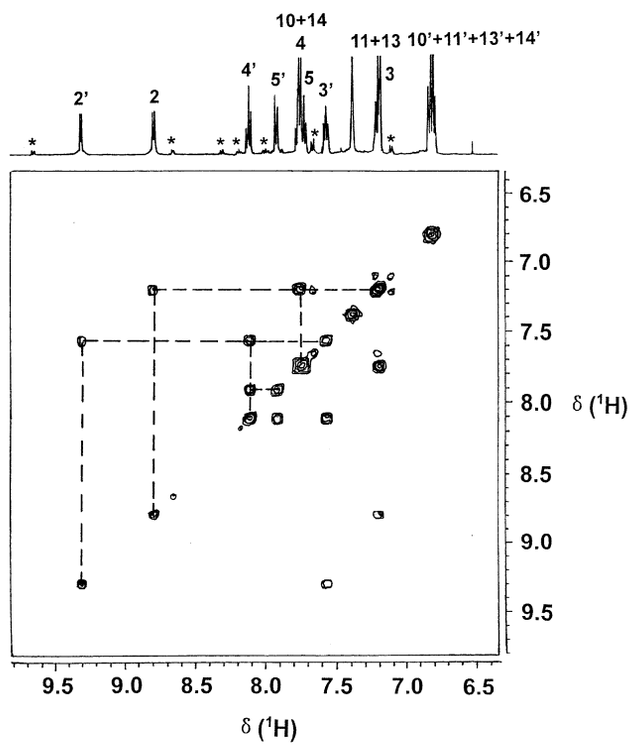


**Fig. 8** The 2D COSY NMR spectrum of complex **1** recorded 48 h after the addition of LiCl (50 mM). The peaks labeled * may correspond to the formation of complex **3** and free ligand.

2D COSY NMR spectrum for **1** recorded 48 h after the addition of LiCl (in a mixture of $CD_3OD/CDCl_3$ in 1 : 4 ratio). The major peaks can be assigned to complex **2** and their chemical shifts are listed in Table 5 (see Scheme 1 for the numbering of the positions). It is noted that small peaks started to appear in the spectrum (Fig. 8) and they are labeled with an asterisk. These peaks increased in intensity with time and became dominant species after 1 week. These are tentatively assigned to complex **3** and free ligand (Scheme 1) as identified by the ESMS.

## *In vitro* antitumor activity

Complexes **1** and **2** demonstrated different antitumor activity *in vitro*. Fig. 9 shows the inhibitory rate of complexes **1** and **2** against HL-60, BEL-7402, P388 and A-549 tumor cell lines. As can be seen, complex **1** was found to be inactive against the above cell lines, while complex **2** demonstrated notable activity against those cell lines. Complex **2** is effective at a concentration of $10^{-5}$ mol $l^{-1}$ against HL-60, BEL-7402 and A-549, tumor cell lines and the antitumor activity decreases to zero after the

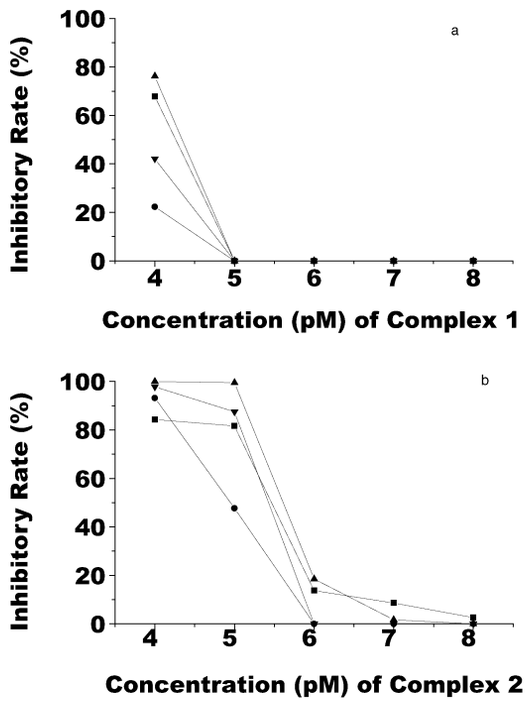


**Fig. 9** Cytotoxic activity of complex **1** (a) and complex **2** (b) against selected tumor cell lines (pM as −log molarity) [■ human leukaemia cells (HL-60), ▲ murine leukaemia cells (P388), ● human liver cancer cells (BEL-7402), ▼ human lung cancer cells (A-549)].

concentration of complex **2** was diluted to $10^{-8}$ mol $l^{-1}$. In HL-60, BEL-7402, P388 and A-549 cells, the growth inhibitory rates of complex **2** were 81.7, 47.7, 99.5 and 87.5%, respectively, whereas those of complex **1** were all 0.0%, at the same concentration of $10^{-5}$ mol $l^{-1}$. We also found that complex **2** exerted similar *in vitro* antitumor activities to cisplatin, a clinically-used metal-containing antitumor drug, in our test system. Additionally, their growth inhibition was in a dose-dependent manner as can be seen in Fig. 9.

## Summary

In this work we have synthesised three novel Pt(II) complexes with a pyridine carboxamide ligand HL. The formation of complex **1**, **2** or **3** is dependent on the absence or presence of chloride (Scheme 1). Two of the three complexes have been structurally characterised. In complex **1** the two ligands chelated to Pt(II) are in a *cis* configuration, while in complex **2** one chelate ring is opened and the two ligands are oriented in a *trans* conformation.

Complex **1** can readily undergo a chelate ring-opening reaction to give complex **2** in the presence of $Cl^-$, whereas complex **2** can undergo ring-closure to give complex **1** in the absence of $Cl^-$. Complex **2** can react further with $Cl^-$ to give complex **3**, although the process is rather slow compared to the first step. As can be seen, complex **3** has the same structural character as cisplatin, and therefore should have the potential to bind to DNA. Preliminary cytotoxicity data show that complex **2** demonstrated similar activity to cisplatin against HL-60 cell lines. This work provides a new strategy in the design of platinum compounds in which the coordination sphere can be controlled by a biological anion.

## Acknowledgements

We are grateful for financial support from the National Natural Science Foundation of China for the Distinguished Young Scientists Fund (Grant No. 29925102) and the Major State Basic Research Development Program (Grant No. G200007750). One of us (Z. G.) is grateful for the support from the Cheung Kong Scholar Program. The authors would like to thank Mr Yong-Jiang Liu and Mr Hua-Qin Wang (Nanjing University) for providing the X-ray structural determinations, and Mr Chenghui Xu and Ms Weiyi Yang for conducting the cytotoxicity assays.

## References

1 B. Rosenberg, L. Van Camp and T. Krigas, *Nature (London)*, 1965, **205**, 698.
2 Special issue on medicinal inorganic chemistry, *Chem. Rev.*, 1999, 99(9).
3 Z. Guo and P. J. Sadler, *Angew. Chem., Int. Ed.*, 1999, **38**, 1512.
4 Z. Guo and P. J. Sadler, *Adv. Inorg. Chem.*, 2000, **49**, 183.
5 E. Wong and C. M. Giandomenico, *Chem. Rev.*, 1999, **99**, 2451.
6 *Cisplatin-Chemistry and Biochemistry of a Leading Anticancer Drug*, ed. B. Lippert, Wiley-VCH, Weinheim, 1999.
7 J. F. Holford, S. Y. Sharp, B. A. Murrer, M. Abrams and L. R. Kelland, *Br. J. Cancer*, 1998, **77**, 366.
8 F. I. Raynaud, F. E. Boxall, P. M. Goddard, M. Valenti, M. Jones, B. A. Murrer, M. Abrams and L. R. Kelland, *Clin. Cancer Res.*, 1997, **3**, 2063.
9 J. F. Holford, F. I. Raynaud, B. A. Murrer, K. Grimaldi, J. A. Hartley, M. J. Abrams and L. R. Kelland, *Anti-Cancer Drug Des.*, 1998, **13**, 1.
10 Y. Chen, Z. Guo, S. Parsons and P. J. Sadler, *Chem. Eur, J.*, 1998, **4**, 672.
11 Y. Chen, J. A. Parkinson, Z. Guo, T. Brown and P. J. Sadler, *Angew. Chem., Int. Ed.*, 1999, **38**, 2060.
12 M. Van Beusichem and N. Farrell, *Inorg. Chem.*, 1992, **31**, 634.
13 U. Bierbach, Y. Qu, T. W. Hambley, J. Peroutka, H. L. Nguyen, M. Doedee and N. Farrell, *Inorg. Chem.*, 1999, **38**, 3535.
14 N. Farrell, *Met. Ions Biol. Syst.*, 1996, **32**, 603.
15 N. Farrell, T. T. B. Ha, J. P. Souchard, F. L. Wimmer, D. Cros and N. P. Johnson, *J. Med. Chem.*, 1989, **32**, 2240.
16 N. Farrell, in *Platinum and other Metal Coordination Compounds in Cancer Chemotherapy*, ed. S. B. Howell, Plenum Press, New York.
17 (*a*) F. Basolo and R. G. Pearson, *Mechanism of Inorganic Reactions*, Wiley, New York, 1967, ch. 5; (*b*) R. G. Wilkin, *Kinetics and Mechanism of Reactions of Transition Metal Complexes*, VCH, Weinheim, 1991, ch. 4.
18 B. Brønnum, H. S. Johansen and L. H. Skibsted, *Inorg. Chem.*, 1992, **31**, 3023.
19 A. Habtemariam and P. J. Sadler, *Chem. Commun.*, 1996, 1785.
20 A. Habtemarian, J. A. Parkinson, N. Margiotta, T. W. Hambley, S. Parsons and P. J. Sadler, *J. Chem. Soc., Dalton Trans.*, 2001, 362.
21 A. Habtemarian, B. Watchman, B. S. Potter, R. Palmer, S. Parsons, A. Parkin and P. J. Sadler, *J. Chem. Soc., Dalton Trans.*, 2001, 1306.
22 N. Margiotta, A. Habtemarian and P. J. Sadler, *Angew. Chem.*, 1997, **36**, 1185.
23 G. B. Kauffman and D. O. Cowan, *Inorg. Synth.*, 1963, **7**, 240.
24 J. A. Yergey, *Int. J. Mass Spectrom. Ion Phys.*, 1983, **52**, 337.
25 S. Dutta, S. Pal and P. K. Battacharya, *Polyhedron*, 1999, **18**, 2157.
26 W. H. Leung, J. X. Ma, V. W. W. Yam, C. M. Che and C. K. Poon, *J. Chem. Soc., Dalton Trans.*, 1991, 1071.
27 G. M. Sheldrick, SHELXTL, Structure Determination Software Programs, Version 5.10, Bruker Analytical X-ray Systems Inc., Madison, WI, USA1997; C. K. Johnson, ORTEP, Report ORNL-5138, Oak Ridge National Laboratory, Oak Ridge, TN, 1976.
28 M. C. Alley, D. A. Scudiero, A. Monks, M. L. Hursey, M. J. Czerwinski, D. Fine, B. J. Abbott, J. G. Mayo, R. H. Shoemaker and M. R. Boyd, *Cancer Res.*, 1988, **48**, 589.
29 P. Skehan, R. Storeng, D. Scudiero, A. Monks, J. McMahon, D. Vistica, J. T. Warren, H. Bokesch, S. Kenney and M. R. Boyd, *J. Natl. Cancer Inst.*, 1990, **82**, 1107.
30 J. Y. Zhang, Q. Liu, Y. Xu, Y. Zhang, X. Z. You and Z. J. Guo, *Acta Crystallogr., Sect. C*, 2001, **57**, 109.
31 R. S. Chapman, F. S. Stephens and R. S. Vagg, *Inorg. Chim. Acta*, 1980, **43**, 29.
32 F. S. Stephens and R. S. Vagg, *Inorg. Chim. Acta*, 1986, **120**, 165.